A Molecular Basis for Advanced Materials in Water Treatment

Randall T. Cygan, C. Jeffrey Brinker, May D. Nyman, Kevin Leung, and Susan B. Rempe

Abstract

A molecular-scale interpretation of interfacial processes is often downplayed in the analysis of traditional water treatment methods; however, such a fundamental approach is perhaps critical for the realization of enhanced performance in traditional desalination and related treatments, and in the development of novel water treatment technologies. Specifically, we examine in this article the molecular-scale processes that affect water and ion selectivity at the nanopore scale as inspired by nature, the behavior of a model polysaccharide as a biofilm, and the use of cluster-surfactant flocculants in viral sequestration.

Introduction

The past 20 years have seen only nominal improvements in the flux of polymeric reverse-osmosis (RO) membranes, in which, by exceeding the osmotic pressure of a saltwater solution, water is transported against concentration gradients through a semipermeable membrane that removes most salts. These improvements have relied on engineering solutions (for example, corrugation of the membrane to enhance its effective surface area) rather than improving material properties to increase flux and selectivity of the membrane itself. The same can be said for ion exchangers, a related class of materials that are proven for both RO membranes and brackish water desalination through ion exchange and can be tuned for specific toxic elements such as lead, selenium, and radionuclides. Further progress in desalination demands a scientific understanding of the water–membrane interface and the transport of water molecules in confined geometries. Only then can membranes be intelligently engineered for both high chemical selectivity and fast transport of pure water. Several examples of water treatment studies that incorporate a molecular-based strategy are discussed in the following sections.

Novel Nanoporous Biomimetic Silica-Based Membranes

The permeation and exclusion of salt in nano-confined aqueous media are central to both selective ion transport and purification/desalination of seawater and brackish water. Recently, highly ordered, nanoporous, silica thin films with tailor-made interior pore surfaces have been synthesized.[1–3] These membranes can be exploited as experimental platforms that help elucidate the roles of pore surface chemistry and confinement on salt hydration and permeation.

The design of efficient ion-exclusion membranes may benefit from the study of biology. For example, the aquaporin transmembrane channels present in our kidneys utilize their unique structural motifs to achieve high water flux and quantitative rejection of Na^+ and Cl^- ions with only small pressure gradient and energy input.[4] Other transmembrane channels, such as the potassium channels of nerve and muscle, are designed to permit rapid permeation of only select ions.[5] Harnessing these basic physical and biomimetic principles will potentially lead to robust solid-state membranes in RO processes, a water purification technology essential to solving water shortage problems in the 21st century. In this section, we briefly describe our combined experimental[1–3] and multiscale modeling[6–8] exploration of the structure–function relationship pertinent to this effort. We note that electrolyte transport in synthetic nanopores has been a subject of experimental[9,10] and modeling[11–13] work elsewhere, but that water treatment has not been a main focus of this research except in zeolite membranes,[14] where the pore diameter is much smaller. In contrast to our own work,[7,15] early efforts to understand the determinants of rapid permeation of select ions in biological channels[5] do not apply quantum mechanical methods principally to interrogate ion selectivity in the interior binding sites of potassium channels.

Figure 1a illustrates the thermodynamic conditions under which various ordered mesophases appear within the surfactant–water–oil detergent phase diagram. In our work, polysilicic acid is included as a secondary hydrophilic component and the evaporation-induced self-assembly technique we pioneered[1] is used to direct the formation of thin-film silica mesophases on porous supports with cubic or bicontinuous nanostructures. Surfactant calcinations or extraction results in mesoporous films characterized by a continuous 3D network of connected pores with ~2–3 nm diameters (depending on choice of surfactant template). Both the pore interior and the thin film ("membrane") surfaces can be functionalized to achieve design functions. For example, we have previously synthesized hybrid organic–inorganic thin films with an approximately 2/nm^2 surface density of $-(CH_2)_3NH_2$ groups. They have been characterized using Fourier-transform infrared (FTIR), transmission electron microscopy (TEM), and grazing-incidence small-angle x-ray scattering (GISAXS) techniques, and have been successfully demonstrated as selective nitrogen gas permeation membranes.[2] A high-resolution TEM image depicting the highly ordered 2-nm diameter pore structure is shown in Figure 1b.

We have also applied plasma-assisted atomic layer deposition (ALD) to coat the

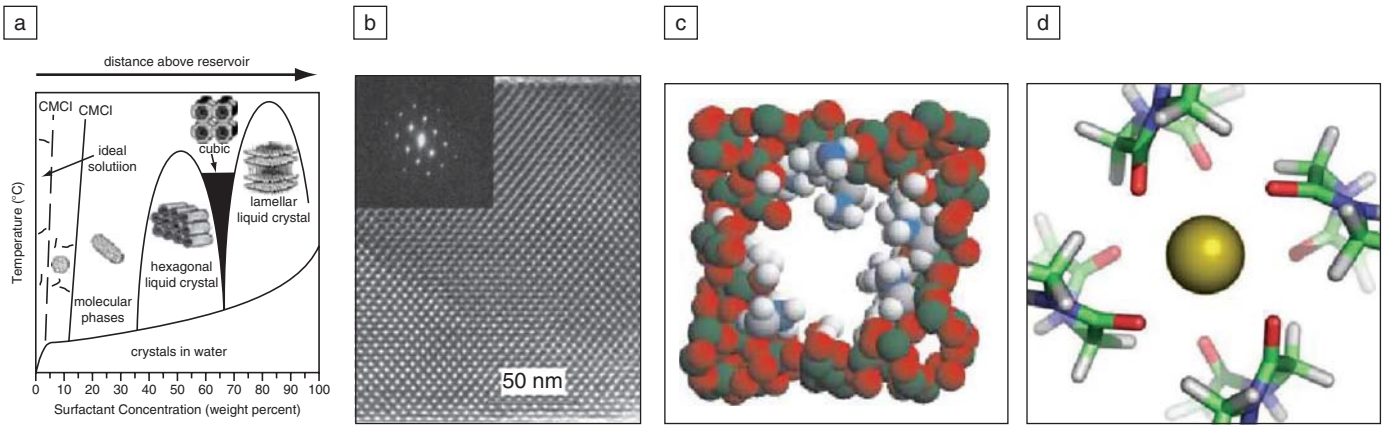

Figure 1. (a) Synthetic phase diagram for porous silica membranes.[1] (b) Transmission electron micrographs of nanoporous silica thin films depicting the highly ordered 2-nm-diameter pore structure.[1] (c) Snapshot of *ab initio* molecular dynamics simulation of $-CH_2NH_2$ functionalized silica nanopore; protons are almost quantitatively transferred from silanol to the amine groups.[6] (H_2O molecules omitted for clarity.) (d) 8-carbonyl binding site made of diglycine molecules and occupied by a permeant K^+ ion from quantum chemical study of a biological potassium channel.[7]

pore surface of silica membranes with silicon dioxide or titanium oxide.[3] This technique yields precisely controlled pore diameters, and its utility has been demonstrated in sealing membrane surfaces in order to synthesize low-*k* dielectric materials for optoelectronic applications.[3] But ALD treatment of silica membranes, combined with organic group functionalization, has the potential to create extremely versatile and well-controlled patch-clamp platforms. Patch-clamp techniques are used traditionally to measure ion transport rates through individual biological ion channels. Our platform allows measurements of ion currents through synthetic nanopores. These platforms will for the first time allow systematic investigations of the effect of pore diameter, structure, and chemistry on water flux, ion permeation, and ion exclusion as functions of the pressure gradient across the membrane. The resulting insight will help the design of the next generation of robust, solid-state RO membranes for large-scale desalination purposes.

To accompany the experiments, we have also conducted simulations of water-filled silica nanopores.[16] Our theoretical work has emphasized highly accurate density functional theory (DFT) calculations. DFT explicitly accounts for the valence electrons of both water and solid substrates, and has proved successful in predicting chemical reactions in water and the electronic polarizability of materials. Thus, we have applied the *ab initio* molecular dynamics (AIMD) technique, which propagates MD trajectories using DFT-derived forces, to examine the surface chemistry of narrow (~1.2-nm-diameter) pores (Figure 1c). Under conditions that are close to room temperature, no chemical reactions are observed in water-filled hydroxylated silica pores. However, at the pH of zero charge (the aqueous solution pH at which the material has on average an equal number of positively charged and negatively charged surface sites and thus becomes electrostatically charge neutral), model silica pores functionalized with $-CH_2NH_2$ groups are found to extract protons from nearby silanol (–SiOH) groups on picosecond time scales and produce positively charged $-NH_3^+$ headgroups that protrude into the pore interior. This leads to large changes in the surface charge distributions. While silanol and amine groups are known to be acidic and basic, respectively, this is a nontrivial finding, because an ammonium group generally requires three water molecules to hydrate it—more than are available inside our narrow model pore. Instead, silanol groups themselves are found to provide a hydrogen bonding environment that stabilizes the $-NH_3^+$ groups.[1]

The consequences of surface chemistry on ion permeation are significant. Using classical force fields fitted with DFT-derived electrostatic potentials, hydroxylated silica pores are found to be intrinsically attractive to Na^+ and repulsive to Cl^-, even at the pH of zero charge. Amine-group–functionalized pores exhibit the opposite trend, favoring anions while also introducing ion traps at the pore surface.[6] This is due to the electrostatic dipole distribution on the pore interior surface and is reminiscent of the carbonyl dipole layer in the narrow filter region of high-selectivity biological potassium channels (see Figure 1d), which allows K^+ ions to pass through rapidly.[5]

The mechanism for potassium channel ion selectivity, which not only differentiates between cations and anions, but also differentiates between small and large cations, is found to be dependent on other parameters as well. Quantum chemical studies[7,15] indicate that rapid, selective K^+ transport combined with exclusion of the smaller Na^+ ion arises from binding sites in the filter containing high numbers of carbonyl ligands (>6) and surrounded by a special local environment electrostatically equivalent to a low-dielectric phase. While no restrictions on the binding site cavity size are necessary, limitations on ligand flexibility are required to maintain high ion coordinations.

Properties of the channel change with alterations in the number of ion-coordinating ligands. Reduction in coordination can occur when chemical groups, specifically hydrogen-bond donors, in the nearby environment compete with an ion for its ligands. Further, selectivity is significantly reduced in binding sites with fewer ion-coordinating ligands. This implies that selectivity of a channel can be tuned, either by modifying the local solvation phase or the binding site itself such that the high ion coordinations necessary for highly selective channels are no longer enforced.[7,8,15] A complete mechanistic view of ion permeation will treat not only properties in and around pore binding sites, but also properties on the membrane surface. These mechanistic predictions will be tested and exploited using functionalized synthetic silica pores; they demonstrate the utility of AIMD and DFT

simulations on water-filled, complex, hybrid, organic–inorganic nanopores.

Finally, we have used DFT to compute the intrinsic energies of Na^+ and Cl^- inside metallic carbon nanotube (CNT) arrays.[16] We predict large binding energies, on the order of an electronvolt, due to the nanotube electronic polarizability. This effect is missing in almost all classical force-field simulations, which instead predict small binding energies and that ions are excluded inside narrow water-filled CNTs. This example emphasizes the importance of incorporating electronic structure effects when modeling the ion permeability in artificial synthetic nanoporous membranes.

Molecular Models for Biofilms and Organic Fouling

Alginate is a relatively simple compound that represents the complex chemistries and structures associated with natural microbial extracellular polymeric substances (EPSs). Microbial exudates typically include straight chains of polysaccharide material that are structurally complex and extremely difficult to characterize. With time, EPSs exuded by microorganisms often result in the formation of biofilms that can associate with polyamide and polyimide materials and ultimately reduce the efficacy of the RO and nanofiltration processes. Organic fouling accelerates the deterioration of the membrane materials and significantly shortens the membrane life.[17,18] Recent experimental and theoretical studies have attempted to elucidate the binding mechanisms of alginate to various cations and to organic membranes.[20,24] In particular, divalent cations such as Ca^{2+} react with the exudate to form metalorganic complexes which create a highly compacted fouling layer that ultimately leads to substantial reduction in permeate flux.[18–19,23]

Alginic acid is a straight-chain, hydrophilic, colloidal, polyuronic acid typically arranged in three combinations of disaccharide subunits (mannuronic, *M*; guluronic, *G*). Approximately 20–50% of polysaccharides produced in a wide sampling of marine and terrestrial bacteria were uronic acids.[25] Alginic acid is a dominant environmental polymer produced by seaweed in marine environments and by environmental bacteria including *Azotobacter vinelandii* and *Pseudomonas aeruginosa*.[26,27] The deprotonated alginate ion complexes aqueous cations including Ca^{2+} and binds to membrane functional groups, although the exact mechanisms are not well understood. The structural flexibility of the alginic acid (or alginate) polymer is the result of torsions (measured as angles ϕ and ψ) about the ether linkage that exists between disaccharide subunits.[24] Functional groups such as carboxylate and alcohol groups on either subunit will inhibit the torsions and limit the number of possible polymer conformers. Ultimately, the proportion of *MM* and *GG* subunits and their macromolecular conformation will determine the affinity of alginate for cation binding.

Molecular simulations using both classical and electronic structure methods have determined the relative stability of various alginic acid and alginate structures, and the optimum binding sites and binding energy of each structure with Ca^{2+}.[24] Figure 2 presents some of the simulation results from an analysis of disaccharide structures and 20-unit polymer chains. Optimum binding of Ca^{2+} is observed for the *GG–D* conformation (one of several initial configurations), which is consistent with the egg-box model proposed previously for gelation processes involving alginate and related polysaccharides.[28] To date, limited effort has been expended on investigations of the more complex nature of organic fouling (biofilms and natural organic matter) of polyamide RO membranes.

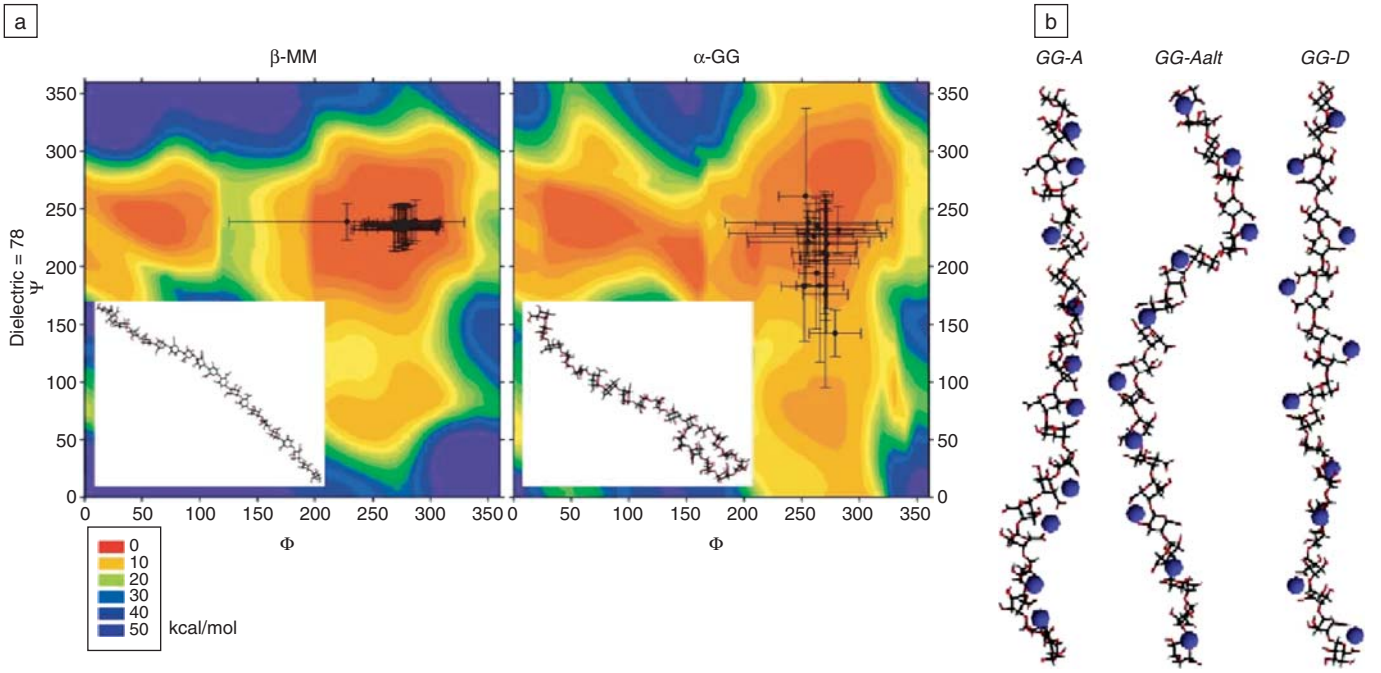

Figure 2. (a) Potential energy maps of the variation in the torsion angles associated with the ether linkage of two 20-unit polysaccharides (*MM* and *GG* alginic acids) derived from molecular simulation using a dielectric value consistent with an aqueous environment.[24] The error bars denote the variation of the torsion angles during a 300 K molecular dynamics simulation. The insets show the final conformation of the polymer at the end of the simulation. (b) Energy-optimized configurations of three *GG* alginate 20-unit polymers associated with calcium ions, derived from molecular simulation.[24]

However, recent atomic force microscopy (AFM) measurements of adhesion forces between membrane or organic foulants and a modified AFM tip have provided considerable evidence toward elucidating the detailed mechanisms and interactions.[29,30] It would be beneficial to provide a theoretical basis using appropriate molecular models to validate these experimental findings and to probe possible membrane modifications that may mitigate organic fouling.

Cluster-Surfactant Flocculent Chemistry for Treatment of Viruses

Cluster-surfactant flocculants for virus sequestration are composed of inorganic metal-oxo polynuclear ions plus surfactants or amphiphiles of an opposite charge. Separately as salts or acids, the components are hydrophilic and water-soluble, but when combined, they form a hydrophobic floc, or precipitate, that is capable of sequestering and separating contaminants such as viruses from aqueous media. The precipitation of the floc occurs via self-assembly of the cluster and surfactant components. The floc components generally assemble to form lamellae of interdigitated surfactant tails alternating with layers of inorganic clusters that are associated with charged surfactant heads. The lamellae range from flat ordered layers to buckled and distorted layers, to complete spherical enclosure of the clusters by a hydrophobic surfactant layer (Figure 3).[31–34]

The variation in cluster-surfactant ordering is influenced by cluster charge, size, and geometry, surfactant tail length, and surfactant charge. These characteristics can be varied in order to optimize virus sequestration ability. Understanding and optimizing the virus sequestration processes may impact a number of applications where removal of viruses from aqueous media is desired, including water re-use, water clarification (alum or ferric process), wastewater treatment, detection, and diagnostics.

We have investigated virus sequestration capabilities of cluster-surfactant phases that contain (1) cationic clusters plus anionic surfactants or (2) anionic clusters plus cationic surfactants. The main cationic cluster of interest is the ε-Keggin aluminum tridecamer, $[Al_{13}O_4(OH)_{24}(H_2O)_{12}]^{7+}$ (Al_{13}^{7+}), a component of the alum flocculation process that plays a key role in the effective removal of a variety of contaminants including microorganisms and anthropogenic organic pollutants.[35–49] This cluster is combined with sodium dodecylsulfate (SDS), an anionic surfactant, or soluble silicate plus cationic surfactant dodecyltrimethylamine ($C_{12}Si$). Anionic clusters known as polyoxometalates (POMs) are based on early d^0 transition metals including W, Nb, Mo, and V. POMs included in this study are $[Nb_6O_{19}]^{8-}$ (Nb_6), $[SiW_{11}O_{39}]^{8-}$ (SiW_{11}), $[PW_{12}O_{40}]^{3-}$ (PW_{12}), and $[SiW_{12}O_{40}]^{4-}$ (SiW_{12}). These are coupled with the cationic surfactants hexadecyltrimethylammonium chloride ($C_{16}Cl$), dodecyltrimethylammonium bromide ($C_{12}Br$), or $C_{12}Si$.

In a typical experiment to test virus sequestration efficacy of a cluster-surfactant floc, the water-soluble components (10^{-6}–10^{-4} molar concentration) are added to an aqueous medium that is spiked with a virus titer (bovine enterovirus, BEV, or influenza A; a representative non-enveloped and enveloped virus, respectively). The precipitate forms, adhering and enmeshing the viruses in the process, and is subsequently filtered. The aqueous medium is then analyzed by *r*RT-PCR (reverse transcriptase polymer chain reaction) for virus concentration remaining. Virus sequestration efficacy of a series of cluster-surfactant phases is summarized in the bar graph of Figure 4a.[50] Overall, these results indicate that: (1) the efficacy of the POM-surfactant phases depends more on the surfactant than the cluster and the order of POM-surfactant efficacy is POM-$C_{12}Si$ > POM-C_{12} > POM-C_{16}; (2) for Al_{13}^{7+}, the $C_{12}Si$ is much more effective than either SDS or NaOH (analogous to alum flocculation). Cluster-surfactant colloids were characterized in aqueous media by dynamic light scattering (DLS) and in the solid-state by powder x-ray diffraction. These results show that larger colloids (Figure 4b) and poorer long-range ordering of the clusters and surfactants corresponded with better virus sequestration efficacy. It is somewhat surprising that the more hydrophobic C_{16} surfactant forms more soluble and less effective virus sequestration phases with a smaller average colloid size than the less hydrophobic C_{12} when combined with POMs. The POM-C_{16} phases also exhibit better long-range order than POM-C_{12} phases. We attribute these results to the better interdigitating ability of C_{16} compared with C_{12}. This results in more ordered precipitates in the solid state and probably offers stabilization in aqueous solution. On the other hand, the shorter C_{12} chain cannot interdigitate as well, and thus more readily precipitates with the POM since the hydrophobic tail region has more contact with the aqueous medium.[50]

Overall, the Al_{13}^{7+}-$C_{12}Si$ and the POM-$C_{12}Si$ flocculants are most effective for virus sequestration, reducing the virus titer of both influenza A and BEV to below the detection limit by *r*RT-PCR (10^1 virus/ml). The dissolved silicate polymerizes with the Al_{13}^{7+} cluster to form anionic aluminosilicate clusters that then precipitate with the cationic surfactants. The role of the dissolved silicate is not clear in the case of the POM-$C_{12}Si$ flocculants, since silicate is not a significant component of the precipitates. Perhaps it serves to slow down the precipitation of the floc since $C_{12}Si$ is stable in aqueous solution, and thus allows more complete adhesion and enmeshment of the viruses.

Ongoing challenges of this work are both fundamental and applied. The Al_{13}^{7+}-$C_{12}Si$ flocculent, along with the hypothetical analogous Fe_{13}^{7+}-$C_{12}Si$, are related to alum or ferric flocculent chemistries utilized in municipal water

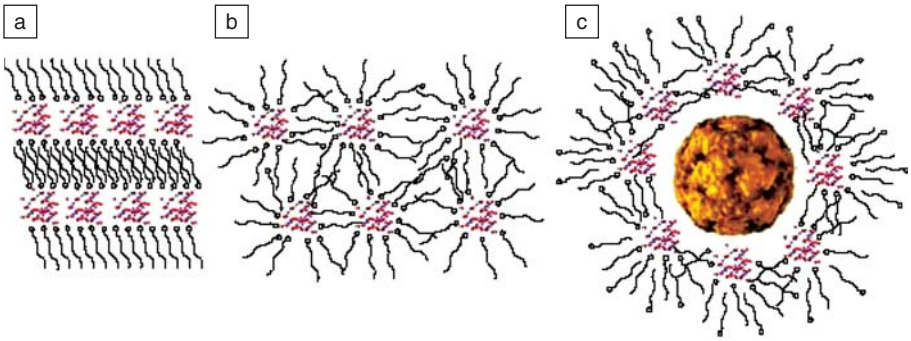

Figure 3. Schematic illustrations of cluster-surfactant self-assembled phases, using the Al_{13} ε-Keggin ion for illustration. (a) A well-ordered phase with alternating layers of clusters and interdigitated surfactant tails. (b) A phase with clusters completely enclosed by surfactants and the enclosed clusters ordered in approximate layers. The assembly in (a) is formed with lower-charged clusters (i.e., ≤ 4) while the assembly in (b) is formed with higher-charged clusters. (c) A cluster-surfactant phase enmeshing a virus (bovine enterovirus).

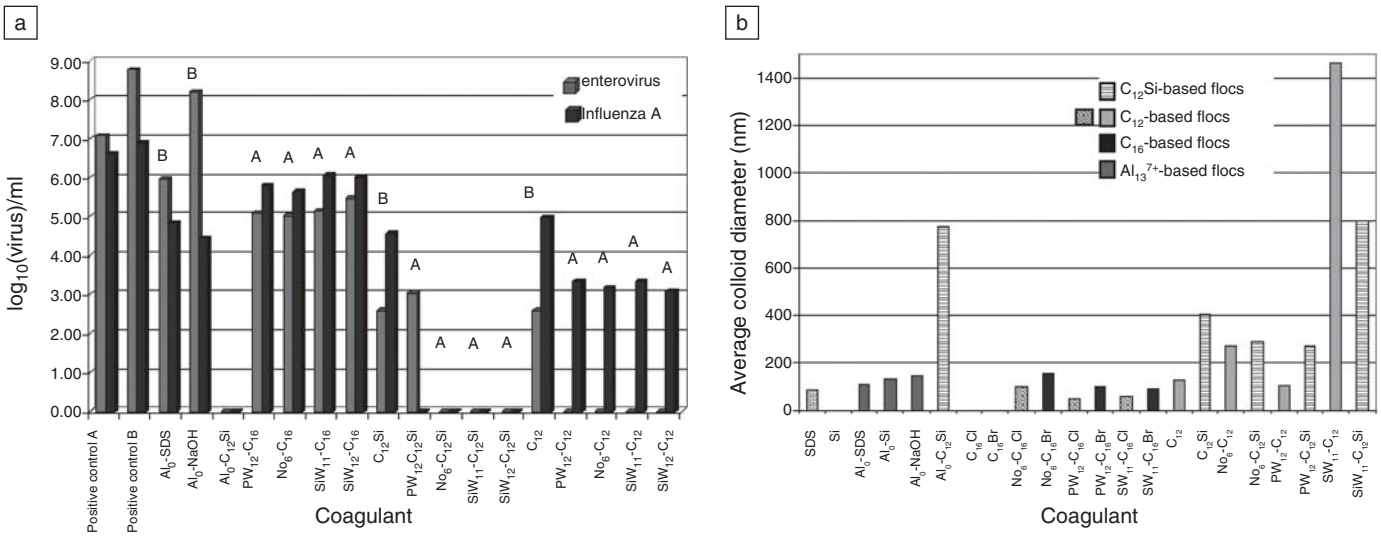

Figure 4. (a) Graph showing the efficacy of various cluster-surfactant phases via concentration of virus remaining in solution, post-coagulation treatment, and filtration.[50] Detection limit of virus by *r*RT-PCR is 10^1 TCID50/ml (tissue culture infectious dose). Positive controls A and B are the initial virus concentrations without treatment. The concentration of each inorganic cluster is 10^{-6} M. (b) Average colloidal diameter of cluster-surfactant phases in aqueous solution determined by dynamic light scattering. The concentration of the inorganic cluster is 10^{-5} M for each experiment.

treatment plants, and will be investigated in further detail for practical use in water treatment applications with improved pathogen removal capabilities. Other ongoing studies involve probing the interactions of viruses with individual floc components (clusters, surfactants, dissolved silicate) to discern enmeshment and adhesion mechanisms of virus sequestration, and to also explore selectivity for specific viruses in the interest of detection technologies.

Acknowledgments

This work was fully funded by the Sandia National Laboratories Laboratory Directed Research and Development program and the U.S. Department of Energy Basic Energy Sciences program. Sandia National Laboratories is a multiprogram laboratory operated by Sandia Corporation, a Lockheed Martin Company, for the U.S. Department of Energy's National Nuclear Security Administration under contract DE-AC04–94AL85000.

References

1. C.J. Brinker, Y.F. Lu, A. Sellinger, H.Y. Fan, *Adv. Mater*. **11**, 579 (1999).
2. N.G. Liu, R.A. Assink, B. Smarsly, C.J. Brinker, *Chem. Commun*. **10**, 1146 (2003).
3. Y.-B. Jiang, N. Liu, H. Gerung, J.L. Cecchi, C.J. Brinker, *J. Am. Chem. Soc*. **128**, 11018 (2006).
4. S. Holmann, S. Nielsen, P. Agre, *Aquaporins* (Academic Press, San Diego, 2001).
5. B. Hille, *Ionic Channels of Excitable Membranes* (Sinauer Associates, Sunderland, MA, ed. 3, 2001).
6. K. Leung, S.B. Rempe, C.D. Lorenz, *Phys. Rev. Lett*. **96**, 095504 (2006).
7. S. Varma, S.B. Rempe, *Biophys.* J. **93**, 1093 (2007).
8. P.C. Jordan, *Biophys.* J. **93**, 1091 (2007).
9. J. Goldberger, R. Fan, P.D. Yang, *Acc. Chem. Res*. **39**, 239 (2006).
10. F.H.J. van der Heyden, D. Stein, K. Besteman, S.G. Lemay, C. Dekker, *Phys. Rev. Lett*. **96**, 224502 (2006).
11. G. Hummer, *Mol. Phys*. **105**, 201 (2007).
12. E.R. Cruz-Chu, A. Aksimentiev, K. Schulten, *J. Phys. Chem. B* **110**, 21497 (2006).
13. C.Y. Won, N.R. Aluru, *J. Am. Chem. Soc*. **129**, 2748 (2007).
14. J.D. Pless, M.L.F. Philips, J.A. Voigt, D. Moore, M. Axness, J.L. Krumhansl, T.M. Nenoff, *Industrial. Engr. Chem. Res*. **45**, 4752 (2006).
15. S. Varma, D. Sabo, S.B. Rempe, *J Mol. Bio*. **374** (2007).
16. K. Leung, M. Marsman, *J. Chem. Phys*. **127**, 154722 (2007).
17. S.K. Hong, M. Elimelech, *J. Membr. Sci*. **132**, 159 (1997).
18. A.E. Childress, M. Elimelech, *J. Membr. Sci*. **119**, 253 (1996).
19. W. Yuan, A.L. Zydney, *Desalination* **122**, 63 (1999).
20. C.M. DeRamos, A.E. Irwin, J.L. Nauss, B.E. Stout, *Inorg. Chim. Acta* **256**, 69 (1997).
21. N. Emmerichs, J. Windgender, H.-C. Flemming, C. Mayer, *Int. J. Biol. Macromol*. **34**, 73 (2004).
22. P. Le-Clech, Y. Marselina, Y. Ye, R.A. Stuetz, V. Chen, *J. Membr. Sci*. **290**, 36 (2007).
23. Q.L. Li, Z.H. Xu, I. Pinnau, *J. Membr. Sci*. **290**, 173 (2007).
24. T.D. Perry, R.T. Cygan, R. Mitchell, *Geochim. Cosmochim. Acta* **70**, 3508 (2006).
25. A.F.D. Kennedy, I.W. Sutherland, *Biotechnol. Appl. Biochem*. **9**, 12 (1987).
26. T.A. Davis, F. Llanes, B. Volesky, A. Mucci, *Environ. Sci. Technol*. **37**, 261 (2003).
27. A. Boyd, A.M. Chakrabarty, *J. Ind. Microbiol. Biotechnol*. **15**, 162 (1995).
28. I. Braccini, S. Pérez, *Biomacromolecules* **2**, 1089 (2001).
29. Q. Li, M. Elimelech, *Environ. Sci. Technol*. **38**, 4683 (2004).
30. S. Lee, M. Elimelech, *Environ. Sci. Technol*. **40**, 980 (2006).
31. M. Nyman, D. Ingersoll, S. Singh, F. Bonhomme, T.M. Alam, C.J. Brinker, M.A. Rodriguez, *Chem. Mater*. **17**, 2885 (2005).
32. T. Ito, H. Yashiro, T. Yamase, *Langmuir* **22**, 2806 (2006).
33. D.G. Kurth, P. Lehmann, D. Volkmer, H. Colfen, M.J. Koop, A. Muller, A. Du Chesne, *Chem. Eur.* J. **6**, 385 (2000).
34. D. Volkmer, A. Du Chesne, D.G. Kurth, H. Schnablegger, P. Lehmann, M.J. Koop, A. Muller, *J. Am. Chem. Soc*. **122**, 1995 (2000).
35. B.D. Ballard, A.A. MacKay, *J. Environ. Eng*. **108**, 131 (2005).
36. P. Paton-Morales, F.I. Talens-Alesson, *Colloid Polym. Sci*. **278**, 697 (2000).
37. M. Porras, F.I. Talens, *Sep. Sci. Technol*. **34**, 2679 (1999).
38. F.I. Talens-Alesson, S. Anthony, M. Bryce, *Water Res*. **38**, 1477 (2004).
39. M. Abbaszadegan, B.K. Mayer, H. Ryu, N. Nwachuku, *Environ. Sci. Technol*. **41**, 971 (2007).
40. H.A. Bustamante, S.R. Shanker, R.M. Pashley, M.E. Karaman, *Water Res*. **35**, 3179 (2001).
41. L. Fiksdal, T. Leiknes, *J. Membr. Sci*. **279**, 364 (2006).

42. Y. Matsui, T. Matsushita, S. Sakuma, T. Gojo, T. Mamiya, H. Suzuoki, T. Inoue, *Environ. Sci. Technol*. **37**, 5175 (2003).
43. T. Matsushita, Y. Matsui, N. Shirasaki, Y. Kato, *Desalination* **178**, 21 (2005).
44. M. Suwa, Y. Suzuki, *Water Sci. Tech*. **47**, 45 (2003).
45. B.T. Zhu, D.A. Clifford, S. Chellam, *Water Res*. **39**, 5153 (2005).
46. H.J. Liu, J.H. Qu, C.Z. Hu, S.J. Zhang, *Colloids Surf., A* **216**, 139 (2003).
47. C.Z. Hu, H.J. Liu, J.H. Qu, D.S. Wang, J. Ru, *Environ. Sci. Technol*. **40**, 325 (2006).
48. B.Y. Gao, Q.Y. Yue, B.J. Wang, *Chemosphere* **46**, 809 (2002).
49. D.S. Wang, Z.K. Luan, H.X. Tang, *J. Am. Water Works Assoc*. **95**, 79 (2003).
50. M. Nyman, J.M. Bieker, S.G. Thoma, D.E. Trudell, *J. Colloid Interfac. Sci*., **316**, 968 (2007). □